Bound-state field-theory approach to proton-structure effects in muonic hydrogen

Peter J. Mohr, J. Griffith, and J. Sapirstein

Bound-state field theory approach to proton structure effects in muonic hydrogen

Peter J. Mohr[*]

National Institute of Standards and Technology, Gaithersburg, MD 20899-8420

J. Griffith[†] and J. Sapirstein[‡]

Department of Physics, University of Notre Dame, Notre Dame, IN 46556

A bound-state field theory approach to muonic hydrogen is set up using a variant of the Furry representation in which the lowest-order Hamiltonian describes a muon in the presence of a point Coulomb field, but the origin of the binding field is taken to be three charged quarks in the proton which are modeled as Dirac particles that move freely within a spherical well. Bound-state field theory techniques are used to evaluate one- and two-photon effects. Particular attention is paid to two-photon-exchange diagrams, which include the effect of proton polarizability. In addition, the modification of the electromagnetic self energy of the proton by the electric field of the muon is examined. Finally, the model is used to carry out a calculation of the static electric polarizability of the proton.

PACS numbers: 31.30.jr, 12.39.Ba,31.30.jd

[*] mohr@nist.gov
[†] jgriff8@nd.edu
[‡] jsapirst@nd.edu

I.   INTRODUCTION

One of the simplest ways to model the proton is as three very light quarks confined in a spherical well. Choosing the radius of the well to be 1.2 fm leads to moderately good agreement with experiment for its electromagnetic properties, such as the charge radius, magnetic moment, and static electric and magnetic polarizabilities. This model, a simplified version of the MIT bag model [1], will be referred to in the following as the static-well model. It allows an alternative approach to the calculation of the electromagnetic properties of the proton, generally treated with methods quite different in character, that uses the methods of conventional bound-state QED. The latter theory is characterized by wave functions that satisfy the Dirac equation in an external field along with electron propagators defined in terms of the same field. When the external field is that of a point Coulomb source, a modification of the interaction representation introduced by Furry [2] allows a systematic Feynman diagram treatment of radiative corrections. This approach can also be applied to many-electron systems, and a Feynman diagram treatment of electron-electron interactions is also possible. As will be explained below, the present paper is patterned on a calculation of these interactions in helium-like ions involving two-photon exchange [3].

The approach we will use in this paper was applied some time ago [4] to the computation of the electromagnetic self energy of the proton and neutron. In that work, both the effect of exchange of a photon between quarks along with the electromagnetic self energy of the quarks were evaluated and found to sum to 0.53 MeV for the proton and -0.28 MeV for the neutron for the case of nearly zero-mass quarks. The fact that the proton is lighter than the neutron remains explained by the fact that the down quark is heavier than the up quark, but it is of note that the electromagnetic correction to the mass splitting, -0.81 MeV, is the same order-of-magnitude as the neutron-proton mass difference, 1.2 MeV.

The proton can be studied with electron-scattering experiments, which have a long history of providing information about its properties, in particular the root-mean-square (rms) radius, $r_{\rm p}$. The proton size has recently received considerable attention because of unexpected results for the $2s_{1/2} - 2p_{3/2}$ transition energy of muonic hydrogen [5]. The issue of determining $r_{\rm p}$ from scattering data can be problematic, as extrapolating the slope of the Dirac form factor to $q^2 = 0$ involves a number of assumptions [6]. An alternative approach is to determine the proton size by doing precise measurements of atomic transitions that are sensitive to the effect of the size. The 2010 CODATA result [9] in fact uses this procedure with hydrogen and deuterium, where the experiment and theory are so accurate that the proton size can be inferred with an accuracy comparable to that available from scattering experiments as of 2010.

Because of its smaller size, muonic hydrogen has long been recognized as a system whose spectrum could be used to determine a much more accurate rms radius of the proton than that obtained from hydrogen and deuterium, but the associated experimental obstacles have only recently been overcome. While indeed much more accurate, the result of Ref. [5] for the proton size,

$$r_{\rm p} = 0.841\,84(67)\,{\rm fm}, \tag{1}$$

is significantly smaller than the CODATA result,

$$r_{\rm p} = 0.8768(69)\,{\rm fm}. \tag{2}$$

This discrepancy is referred to as the muonic hydrogen puzzle.

One possible explanation of the puzzle involves the electromagnetic structure of the proton, and the largest theoretical uncertainty comes from an effect called proton polarizability. This is generally evaluated by relating the energy shift to forward virtual photon-proton scattering. The amplitude describing this scattering, $T^{\mu\nu}(\nu, q^2)$, can then be related to proton form factors through dispersion relations. A recent paper that covers all contributions to muonic hydrogen with particular attention to proton polarizability is Ref. [7]; in the conclusion, we compare our results to results quoted in that paper. Another recent summary is given in Ref. [8]. A number of issues involving convergence of the dispersion theory integrals and the need for experimental data complicate that approach. The purpose of the present paper is to provide an alternative analysis patterned after bound-state field theory calculations in atomic physics. This will be done by using the static-well model of the proton together with standard bound-state QED. As we will show, there is a natural way of setting up a consistent QED calculation for hydrogen and muonic hydrogen, with the proton treated as a bound state of three quarks interacting with an electron or a muon, that requires no scattering information for its predictions; rather it depends only on the radius of the well.

Regarding the proton as three relativistic particles confined to a small volume is closely analogous to treating lithium-like highly-charged ions, where the electrons for large nuclear charge Z are quite relativistic and the ion has a size of $1/Z$ Bohr radius. This problem has recently been addressed with techniques similar to those used for helium-like ions mentioned above [3], and have been shown to provide an accurate description of lithium-like ions [10, 11], the spectra of which have been measured with high accuracy [12].

In these calculations almost all of the important physics is described by Feynman diagrams with one or two photons. The same turns out to hold for the present calculation, though in this paper, while we will show all relevant diagrams,

we concentrate our attention on two effects dependent on proton structure, the polarizability of the proton and the screening of the proton electromagnetic self energy.

Our model of the proton is extremely simple, but there are three reasons we have chosen it. The first is that proton structure effects are generally very small, with even the largest, the effect of its finite size, accounting for about 2 percent of the transition energy in muonic hydrogen. Thus even a crude determination of a proton structure effect will have a small relative theoretical error. The second is that while the proton polarizability correction has been evaluated with other methods, a contribution we term the proton Lamb shift has not, and the results presented here may stimulate more sophisticated calculations. The final reason is that mentioned above, to explore a method of calculating the effect of proton structure on atomic energy levels that does not require the use of dispersion theory.

We will in the following consider the effect of proton structure on both electronic and muonic hydrogen. Because our formalism does not include recoil, we will present results in terms of the electron mass m_e and the muon mass m_μ even though reduced-mass effects on the latter are about 10 percent. When we give a general formula, we refer to a lepton with mass m_l. The state of the lepton, in practice either $2s$ or $2p_{3/2}$, will be denoted v, and the index m will be used for sums over intermediate leptonic states: for the corresponding case of quarks, we use g to denote a ground-state quark and reserve n for sums over intermediate quark states.

The plan of the paper is as follows. We begin in Sec. II with a quantum mechanical (QM) treatment of the shift in energy levels arising from the perturbation of replacing the potential of a point proton Coulomb field with that of a general distribution of charge $\rho(\mathbf{r})$. This perturbation theory is evaluated through second order. In Sec. III we turn to a quantum-field-theoretic approach to the problem in the context of the static-well model. We do this by modifying the standard Furry representation [2] through forcing the lowest-order Hamiltonian to be the same as that used in that representation, but having the quarks in the proton provide the Coulomb field instead of assuming a point source. This requires the introduction of a new term in the interaction Hamiltonian we call the counter term, the effects of which however are quite simple to evaluate. We also define the static-well model and briefly review the calculation of the proton electromagnetic self energy. In Sec. IV we use bound-state field theory to treat one-photon exchange, and show that the results agree with the first-order QM energy. We note here that in this paper we use the Coulomb gauge and treat only Coulomb photons for all exchanged photons. For the QM approach this corresponds to ignoring magnetic effects, and in field theory to leaving out transverse-photon exchange. In Sec. V we then turn to two-photon exchange diagrams, which we break into two classes, one in which only one photon attaches to the lepton, with the other being emitted and reabsorbed in the proton, and a second in which each photon is exchanged between the lepton and a quark. In Sec. VI A we treat the first class, which has no QM analog, and present a calculation of the contribution, which we call the proton Lamb shift. In Sec. VI B we treat the second class, but again make a breakup of the diagrams into firstly a part in which the proton is left unchanged, and secondly a part where it is excited. (In our model this means that the spectral representation for the quark propagator is either saturated with the $1s$ state, or else that state is excluded). The first part will be shown to correspond exactly to the second-order QM energy. The second part, the proton polarizability, is then evaluated. The related calculation of the proton's static electric polarizability is carried out in Sec. VII and it is shown that in the $\kappa = 1$ angular momentum channel a complete cancellation between positive- and negative-energy state terms occurs, leaving only contributions from the $\kappa = -2$ intermediate states. In the conclusion we compare our results to the results of other calculations and describe directions for future progress.

II. PERTURBATION THEORY OF FINITE-NUCLEAR-SIZE EFFECTS

We consider a central potential for hydrogen or muonic hydrogen coming from a finite charge distribution $\rho(\mathbf{x})$, normalized to unity. The corresponding static potential is

$$V(\mathbf{x}) = -Z\alpha \int d\mathbf{x}' \, \frac{\rho(\mathbf{x}')}{|\mathbf{x} - \mathbf{x}'|}. \tag{3}$$

While we have $Z = 1$, the following discussion can also be applied to the case $Z \neq 1$. We start with a point-Coulomb binding field, so this distribution leads to the perturbation

$$\delta V(\mathbf{x}) = -Z\alpha \int d\mathbf{x}' \, \frac{\rho(\mathbf{x}') - \delta(\mathbf{x}')}{|\mathbf{x} - \mathbf{x}'|}. \tag{4}$$

The first-order correction,

$$E^{(1)} = \int d\mathbf{x} \phi_v^\dagger(\mathbf{x}) \, \delta V(\mathbf{x}) \, \phi_v(\mathbf{x}), \tag{5}$$

is valid for either a relativistic or nonrelativistic calculation. We first consider the nonrelativistic limit. Then in leading order the wave functions may be replaced by their value at the origin and the first-order energy is

$$E_0^{(1)} = -Z\alpha \, |\phi_v(0)|^2 \int \mathrm{d}\boldsymbol{x} \int \mathrm{d}\boldsymbol{x}' \, \frac{\rho(\boldsymbol{x}') - \delta(\boldsymbol{x}')}{|\boldsymbol{x} - \boldsymbol{x}'|}$$

$$= -Z\alpha \, |\phi_v(0)|^2 \int \mathrm{d}\boldsymbol{x}' \, 4\pi \left(\frac{1}{u^2} - \frac{1}{6} \, \boldsymbol{x}'^2 + \ldots \right) [\rho(\boldsymbol{x}') - \delta(\boldsymbol{x}')]$$

$$= \frac{2\pi Z\alpha}{3} \, |\phi_v(0)|^2 \int \mathrm{d}\boldsymbol{x} \, \boldsymbol{x}^2 \rho(\boldsymbol{x}) = \frac{2(Z\alpha)^4}{3n^3} \, m_l^3 \int \mathrm{d}\boldsymbol{x} \, \boldsymbol{x}^2 \rho(\boldsymbol{x}), \tag{6}$$

where in the last step we have assumed v to be an ns-state, and u is defined in the following.

The integral over $\mathrm{d}\boldsymbol{x}$ has been carried out using a cutoff procedure which we now describe. We introduce a parameter u, understood to ultimately be taken to zero, and work with the basic identity

$$\int \mathrm{d}\boldsymbol{x} \, \frac{1}{|\boldsymbol{x}_2 - \boldsymbol{x}|} \, \frac{\mathrm{e}^{-u|\boldsymbol{x} - \boldsymbol{x}_1|}}{|\boldsymbol{x} - \boldsymbol{x}_1|} = \frac{4\pi}{u^2} \, \frac{1 - \mathrm{e}^{-u|\boldsymbol{x}_2 - \boldsymbol{x}_1|}}{|\boldsymbol{x}_2 - \boldsymbol{x}_1|}, \tag{7}$$

which for small u has the expansion

$$\int \mathrm{d}\boldsymbol{x} \, \frac{1}{|\boldsymbol{x}_2 - \boldsymbol{x}|} \, \frac{\mathrm{e}^{-u|\boldsymbol{x} - \boldsymbol{x}_1|}}{|\boldsymbol{x} - \boldsymbol{x}_1|} = 4\pi \left(\frac{1}{u} - \frac{1}{2} |\boldsymbol{x}_2 - \boldsymbol{x}_1| + \frac{u}{6} |\boldsymbol{x}_2 - \boldsymbol{x}_1|^2 - \frac{u^2}{24} |\boldsymbol{x}_2 - \boldsymbol{x}_1|^3 + \ldots \right) \tag{8}$$

By differentiating once or twice with respect to u, we have

$$\int \mathrm{d}\boldsymbol{x} \, \frac{\mathrm{e}^{-u|\boldsymbol{x} - \boldsymbol{x}_1|}}{|\boldsymbol{x}_2 - \boldsymbol{x}|} = 4\pi \left(\frac{1}{u^2} - \frac{1}{6} |\boldsymbol{x}_2 - \boldsymbol{x}_1|^2 + \mathcal{O}(u) \right) \tag{9}$$

and

$$\int \mathrm{d}\boldsymbol{x} \, \frac{\mathrm{e}^{-u|\boldsymbol{x} - \boldsymbol{x}_1|}}{|\boldsymbol{x}_2 - \boldsymbol{x}|} |\boldsymbol{x} - \boldsymbol{x}_1| = 4\pi \left(\frac{2}{u^3} - \frac{1}{12} |\boldsymbol{x}_2 - \boldsymbol{x}_1|^3 + \mathcal{O}(u) \right). \tag{10}$$

We have used Eq. (9) in the derivation of Eq. (6), and use Eq. (10) to evaluate the correction coming from the variation of the wave function to leading order. For S states, this arises from

$$|\phi_v(\boldsymbol{x})|^2 = |\phi_v(0)|^2 \left(1 - 2Z\alpha m_l |\boldsymbol{x}| + \ldots \right), \tag{11}$$

which yields an additional contribution of

$$E_1^{(1)} = 2(Z\alpha)^2 m_l \, |\phi_v(0)|^2 \int \mathrm{d}\boldsymbol{x} \, |\boldsymbol{x}| \int \mathrm{d}\boldsymbol{x}' \, \frac{\rho(\boldsymbol{x}') - \delta(\boldsymbol{x}')}{|\boldsymbol{x} - \boldsymbol{x}'|}$$

$$= 2(Z\alpha)^2 m_l \, |\phi_v(0)|^2 \int \mathrm{d}\boldsymbol{x}' \, 4\pi \left(\frac{2}{u^3} - \frac{1}{12} |\boldsymbol{x}'|^3 + \ldots \right) [\rho(\boldsymbol{x}') - \delta(\boldsymbol{x}')]$$

$$= -\frac{2\pi(Z\alpha)^2}{3} \, m_l \, |\phi_v(0)|^2 \int \mathrm{d}\boldsymbol{x} \, |\boldsymbol{x}|^3 \rho(\boldsymbol{x}) = -\frac{2(Z\alpha)^5}{3n^3} \, m_l^4 \int \mathrm{d}\boldsymbol{x} \, \boldsymbol{x}^3 \rho(\boldsymbol{x}). \tag{12}$$

This term cancels a corresponding term in second-order perturbation theory, which is given by the standard form

$$E^{(2)} = \int \mathrm{d}\boldsymbol{x}_2 \int \mathrm{d}\boldsymbol{x}_1 \, \phi_v^\dagger(\boldsymbol{x}_2) \, \delta V(\boldsymbol{x}_2) \sum_{m \neq v} \frac{\phi_m(\boldsymbol{x}_2) \, \phi_m^\dagger(\boldsymbol{x}_1)}{\epsilon_v - \epsilon_m} \, \delta V(\boldsymbol{x}_1) \, \phi_v(\boldsymbol{x}_1). \tag{13}$$

The sum over terms involving m is -1 times the reduced Green function. This expression is again valid for either a relativistic or nonrelativistic calculation. The correction to the potential is only non-zero inside the nucleus, which means that the wave functions and reduced Green function are evaluated for small arguments, because the Bohr radius for both the muon and electron is large compared to the nuclear size. We again take the nonrelativistic limit.

Then the wave functions may be evaluated at the origin and the reduced Green function may be replaced by the nonrelativistic free Green function to give

$$
E_0^{(2)} = -\frac{m_l}{2\pi} |\phi_v(0)|^2 \int \mathrm{d}\boldsymbol{x}_2 \int \mathrm{d}\boldsymbol{x}_1 \, \delta V(\boldsymbol{x}_2) \frac{1}{|\boldsymbol{x}_2 - \boldsymbol{x}_1|} \delta V(\boldsymbol{x}_1)
$$

$$
= -\frac{(Z\alpha)^2 m_l}{2\pi} |\phi_v(0)|^2 \int \mathrm{d}\boldsymbol{x}_2' \int \mathrm{d}\boldsymbol{x}_1'
$$

$$
\times \int \mathrm{d}\boldsymbol{x}_2 \int \mathrm{d}\boldsymbol{x}_1 \frac{\rho(\boldsymbol{x}_2') - \delta(\boldsymbol{x}_2')}{|\boldsymbol{x}_2 - \boldsymbol{x}_2'|} \frac{1}{|\boldsymbol{x}_2 - \boldsymbol{x}_1|} \frac{\rho(\boldsymbol{x}_1') - \delta(\boldsymbol{x}_1')}{|\boldsymbol{x}_1 - \boldsymbol{x}_1'|} . \tag{14}
$$

Introducing cutoffs allows us to carry out the integrals over the unprimed variables with the formulas given above, resulting in

$$
E_0^{(2)} = (Z\alpha)^2 m_l |\phi_v(0)|^2 \int \mathrm{d}\boldsymbol{x}_2' \int \mathrm{d}\boldsymbol{x}_1'
$$

$$
\times \int \mathrm{d}\boldsymbol{x}_1 \, [\rho(\boldsymbol{x}_2') - \delta(\boldsymbol{x}_2')] \, |\boldsymbol{x}_2' - \boldsymbol{x}_1| \frac{\rho(\boldsymbol{x}_1') - \delta(\boldsymbol{x}_1')}{|\boldsymbol{x}_1 - \boldsymbol{x}_1'|} , \tag{15}
$$

and

$$
E_0^{(2)} = -\frac{\pi(Z\alpha)^2 m_l |\phi_v(0)|^2}{3} \left[\int \mathrm{d}\boldsymbol{x}_2 \int \mathrm{d}\boldsymbol{x}_1 \, \rho(\boldsymbol{x}_2) |\boldsymbol{x}_2 - \boldsymbol{x}_1|^3 \rho(\boldsymbol{x}_1) - 2 \int \mathrm{d}\boldsymbol{x} \, |\boldsymbol{x}|^3 \rho(\boldsymbol{x}) \right]
$$

$$
= -\frac{(Z\alpha)^5}{3n^3} m_l^4 \left[\int \mathrm{d}\boldsymbol{x}_2 \int \mathrm{d}\boldsymbol{x}_1 \, \rho(\boldsymbol{x}_2) |\boldsymbol{x}_2 - \boldsymbol{x}_1|^3 \rho(\boldsymbol{x}_1) - 2 \int \mathrm{d}\boldsymbol{x} \, |\boldsymbol{x}|^3 \rho(\boldsymbol{x}) \right]. \tag{16}
$$

As alluded to above, the second term in the square brackets in Eq. (16) is cancelled by Eq. (12). The first term in the square brackets is the third Zemach moment, which we denote $\langle r^3 \rangle_Z$. An interesting feature about this term is that it too is cancelled by a term that arises when the nucleus is allowed to undergo low-energy excitations (proton polarizability), though we will not use this fact directly, and instead just evaluate the entire effect. We turn now to a field-theoretic approach based on the static-well model, and begin by introducing a formalism for bound-state field theory.

III. FORMALISM

While the formalism we use here is to our knowledge novel, it is a simple extension of the Furry representation [2], which we now briefly review. We will use this representation both for leptons and quarks, and begin by describing how it is used for the former. The full QED Hamiltonian used for describing the scattering of free leptons is $H = H_0 + H_\mathrm{I}$, with ($\{\hbar\} = 1, \{c\} = 1, \{e\} = 1$),

$$
H_0 = \int \mathrm{d}\boldsymbol{x} \, \psi^\dagger(x) \left[\boldsymbol{\alpha} \cdot \boldsymbol{p} + \beta m_l \right] \psi(x) \tag{17}
$$

and

$$
H_\mathrm{I} = q_\mathrm{e} \int \mathrm{d}\boldsymbol{x} \, \overline{\psi}(x) \gamma_\mu \psi(x) A^\mu(x), \tag{18}
$$

with $q_\mathrm{e} = -e$. We suppress normal ordering and the self-mass counter term for simplicity. The Furry representation is used when H_0 is replaced by

$$
\tilde{H}_0 = \int \mathrm{d}\boldsymbol{x} \, \psi^\dagger(x) \left[\boldsymbol{\alpha} \cdot \boldsymbol{p} + \beta m_l - \frac{Z\alpha}{|\boldsymbol{x}|} \right] \psi(x). \tag{19}
$$

This builds in a classical Coulomb field from an infinite mass proton. Carrying out a unitary transformation to eliminate $\tilde{H}_0$ rather than H_0 leads to the Furry representation in place of the interaction representation. While the

interaction Hamiltonian H_I of a lepton with photons keeps the same form, the lowest order spectrum now consists of hydrogenic bound and scattering states, and the lepton Green function obeys the relation

$$\left(-i\boldsymbol{\alpha}\cdot\boldsymbol{\nabla_x} + \beta m_l - \frac{Z\alpha}{|\boldsymbol{x}|} - z\right) G(\boldsymbol{x},\boldsymbol{y};z) = \delta(\boldsymbol{x}-\boldsymbol{y}), \tag{20}$$

which has the spectral representation

$$G(\boldsymbol{x},\boldsymbol{y};z) = \sum_m \frac{\phi_m(\boldsymbol{x})\phi_m^\dagger(\boldsymbol{y})}{\epsilon_m - z}. \tag{21}$$

In the present case we treat proton structure using the static-well model to specify the wave functions and Green functions of the constituent quarks. However, the influence of the proton on a lepton in a bound state cannot be treated perturbatively, so we need to build the binding of the lepton into the formalism nonperturbatively. We do this by modifying the breakup of the Hamiltonian given above to $H = (H_0 + H_X) + (H_I - H_X)$. If we choose

$$H_X = -\int d\boldsymbol{x}\, \psi^\dagger(x)\frac{Z\alpha}{|\boldsymbol{x}|}\,\psi(x), \tag{22}$$

then this breakup is $H = \tilde{H}_0 + (H_I - H_X)$. In the following we refer to H_X as the counter term, though of course it is to be distinguished from the electron mass counter term. We stress that we do *not* assume that a classical Coulomb field is present. However, because we have added a new term to the interaction Hamiltonian, $\tilde{H}_0$ is unchanged from the usual Furry representation, and the same wave functions and Green functions used in Feynman diagram calculations in that representation can be used, although extra Feynman diagrams involving H_X need to be included.

The use of the Furry representation must be extended to quarks in order to account for the proton's Coulomb field. In this case H_0 and H_I are almost identical to the free case, but in H_0 we assume the presence of a static well that confines the quarks, the details of which are given below, so that the up and down quark fields are expanded in terms of solutions to the Dirac equation in this well. The proton then consists of the usual two up quarks and one down quark, and the sum of their charges leads to the Coulomb field felt by the lepton.

Since the lowest-order problem describes the basic physics of the atom, there has to be cancellation between diagrams in which a Coulomb photon is exchanged between the lepton and the quarks in the proton and diagrams with one counter term. In second order another cancellation between two-photon exchange diagrams and diagrams involving one and two counter terms must take place, and so on. Because the proton is now modeled as a finite object, the cancellation will not be complete, and we will identify the parts remaining after the near cancellation as the subject of this paper, proton structure effects. It is of course vital for this procedure to make sense that the cancellation not only takes place, but that the perturbation expansion converges. We will present results for the first and second terms in the expansion below. In determining the order of the expansion we note that the counter term H_X is of the same order as two H_Is.

The static-well model has well-known solutions which we show partly to establish notation. We represent the solution to the free Dirac equation in a spherically symmetric well, centered at the same origin as used in Furry representation, by

$$\phi_q(\boldsymbol{r}) = \begin{pmatrix} f_1(r)\chi_{\kappa\mu}(\hat{\boldsymbol{r}}) \\ if_2(r)\chi_{-\kappa\mu}(\hat{\boldsymbol{r}}) \end{pmatrix}. \tag{23}$$

Here $\chi_{\kappa\mu}(\hat{\boldsymbol{r}})$ is a spherical spinor and the radial wavefunctions obey the equations

$$\left(\frac{\partial}{\partial r} + \frac{1+\kappa}{r}\right) f_1(r) - [m(r) + E]\, f_2(r) = 0 \tag{24}$$

$$\left(\frac{\partial}{\partial r} + \frac{1-\kappa}{r}\right) f_2(r) + [E - m(r)]\, f_1(r) = 0. \tag{25}$$

Confinement is enforced by choosing $m(r)$ to be constant inside the well and tending to infinity for $r > R$, which leads to the MIT bag model boundary conditions [1]. The ground-state solution for the case $m(r) = 0$ for $r < R$, which will be used throughout this paper, is

$$f_1(r) = \frac{N}{r}\sin(wx)$$
$$f_2(r) = \frac{N}{r}\left[\cos(wx) - \frac{\sin(wx)}{wx}\right], \tag{26}$$

with $x = r/R$ and

$$N = \frac{1}{\sqrt{R}} \sqrt{\frac{2w^2}{2w^2 + \cos(2w) - 1}}. \tag{27}$$

Here $w = 2.042\,787$ for the ground state, which gives $\epsilon_g = 335.9$ MeV for $R = 1.2$ fm. When this wave function is used for the up and down quarks the second and third moments, which can be calculated analytically, are

$$\langle r^2 \rangle = R^2 \frac{2w^3 - 2w^2 + 4w - 3}{6w^2(w-1)} = R^2\, 0.531\,392 \tag{28}$$

and

$$\langle r^3 \rangle = R^3 \frac{2w^2 - 2w + 3}{8w(w-1)} = R^3\, 0.426\,041. \tag{29}$$

While an analytic form can be derived for the third Zemach moment, it is lengthy and involves the sine integral, so we give only its numerical value,

$$\langle r^3 \rangle_Z = R^3\, 1.280\,621. \tag{30}$$

The wave functions of the up and down quarks are identical in this zero mass case, and we denote them as $\phi_g(\boldsymbol{x})$. This approximation leads to the important simplification that the charge density of the proton, even though it consists of three quarks, can be written in terms of $\phi_g(\boldsymbol{x})$,

$$\rho_g(\boldsymbol{x}) = \phi_g^\dagger(\boldsymbol{x})\phi_g(\boldsymbol{x}). \tag{31}$$

We will see that in our calculations of one- and two-Coulomb photon exchange this density will enter in exactly the same way as it does in Sec. II in parts of the calculation, thereby reproducing the results of that section with the static-well model charge density. Extra terms arising from the field theory approach will be identified with polarizability effects.

Were we to use different masses, the charge densities of the up and down quarks would differ, and in that case we would use

$$\rho_g(\boldsymbol{x}) = \frac{4}{3}\,\phi_u^\dagger(\boldsymbol{x})\phi_u(\boldsymbol{x}) - \frac{1}{3}\,\phi_d^\dagger(\boldsymbol{x})\phi_d(\boldsymbol{x}). \tag{32}$$

The $2s_{1/2}$ and $2p_{3/2}$ atomic wavefunctions for the lepton are the standard Dirac-Coulomb solutions and will be denoted as $\phi_v(\boldsymbol{x})$. As proton structure effects are strongly suppressed for the $2p_{3/2}$ case, even though we will continue to use v in formulas, in practice we will always assume $v = 2s_{1/2}$.

The radius R is the only variable in this calculation, and we will use different values to study the R dependence of what is by far the largest proton structure correction, the finite size correction from one-photon exchange. However, because all other proton structure effects are much smaller, the value 1.2 fm is understood to be used for those corrections.

For the calculation carried out here, which involves a quark propagating in the well, we use the same kind of spectral decomposition as given in Eq. (21),

$$G_q(\boldsymbol{x}, \boldsymbol{y}; z) = \sum_n \frac{\phi_n(\boldsymbol{x})\phi_n^\dagger(\boldsymbol{y})}{\epsilon_n - z}. \tag{33}$$

The sum over m for the lepton and n for the quark Green functions can be carried out using the method of finite basis sets [16], which have been used extensively for atomic calculations, with only minor modifications of the associated computer code required for application to the quark Green function. This is because the atomic calculations were set up in the same kind of confining well as used here, but in that case only for the purpose of discretizing the spectrum, with the well radius chosen to be much larger than the atom or ion being considered.

We will need the explicit form for the spin-up and spin-down proton wave function, with the former being

$$|\,p_\uparrow\rangle = \frac{\epsilon_{ijk}}{\sqrt{72}} \left[-2b_{id}^\dagger b_{ja}^\dagger b_{ka}^\dagger + b_{ic}^\dagger b_{jb}^\dagger b_{ka}^\dagger + b_{ic}^\dagger b_{ja}^\dagger b_{kb}^\dagger \right] |0\rangle. \tag{34}$$

In Eq. (34) a and b denote spin up and down states of an up quark and c and d spin up and down states of a down quark; ϵ_{ijk} is the Levi-Civita symbol, which makes the proton a color singlet after the implicit sum over colors ijk is

carried out. Because we are taking the up and down quark masses equal to zero, the associated wave function $\phi_c(\boldsymbol{x})$ can be replaced by $\phi_a(\boldsymbol{x})$ and $\phi_d(\boldsymbol{x})$ by $\phi_b(\boldsymbol{x})$, which simplifies later formulas. When the spin state of the quark is not important, we simply use $\phi_{\mathrm{g}}(\boldsymbol{x})$.

Energy shifts are calculated with the use of S-matrix techniques, where we use Sucher's generalization of the Gell-Mann Low formula [17],

$$\Delta E = \lim_{\epsilon \to 0,\, \lambda \to 1} \frac{\mathrm{i}\epsilon}{2} \frac{\partial}{\partial \lambda} \ln \left\langle v \left| \mathrm{T}\!\left[e^{-\mathrm{i}\lambda H_{\mathrm{I}}(\epsilon)} \right] \right| v \right\rangle. \tag{35}$$

Here $H_{\mathrm{I}}(\epsilon)$ indicates that a factor $e^{-\epsilon|t|}$ is included in the time integral over the Hamiltonian density in order to adiabatically turn off the interaction at large positive and negative times. The advantage of this formula is that the S-matrix can be described with standard Feynman diagram techniques, with the adiabatic factors usually trivially leading to a factor $1/\epsilon$ that cancels the ϵ in the numerator of the above formula, though when we deal with two-photon diagrams, the formalism is needed to cancel disconnected diagrams. Details of how this works along with other technical issues can be found in Ref. [3]. That work described a calculation of two-photon exchange diagrams contributing to energy shifts of excited states of helium-like ions, but the basic approach is almost identical. The most important difference is that while in that work $|v\rangle$ describes two electrons, here it describes one electron or muon and three quarks, and is given by

$$|v\rangle = b_v^\dagger \, |p\rangle. \tag{36}$$

The diagrams that involve one photon are given in Figs. 1, 2, and 3(a). Fig. 1 is the standard one-loop Lamb shift, which has been evaluated to spectroscopic accuracy. Fig. 2 is the electromagnetic self energy of the proton, which was calculated using the Feynman gauge in Ref. [4]. The simplest diagram to evaluate is Fig. 2(a), photon exchange between pairs of quarks. It contributes -0.222 MeV to the proton electromagnetic self energy, all of which comes from the vector part of the photon exchange. More difficult to calculate is the self-energy diagram of Fig. 2(b). This diagram in general requires the inclusion of a self-mass counter term, though not for the zero mass case. After this subtraction an ultraviolet-divergent vertex term generally remains, but because the quarks move freely within the well the ultraviolet divergent part of this term vanishes, and numerical evaluation yields 0.658 MeV (the results given in Ref. [4] referred to in the introduction are based on the radius $R = 1$ fm, but because they scale as $1/R$ a factor 1.2 must be inserted for comparison to the present work). We note that vacuum polarization terms do not contribute for an isolated proton, but may be of interest for muonic hydrogen, an issue that will be discussed further in the conclusion. Finally, Figs. 3(a) and 3(b) describe exchange of a photon between the lepton and the quarks in the proton and the first-order effect of H_{X} respectively, and we now turn to their numerical evaluation.

IV.   ONE-PHOTON EXCHANGE

We evaluate Fig. 3(a) in the Coulomb gauge, and consider only Coulomb photon exchange. This leads to the energy shift

$$\Delta E_{1\mathrm{C}} = -\alpha \int \frac{\mathrm{d}\boldsymbol{x}\,\mathrm{d}\boldsymbol{y}}{|\boldsymbol{x} - \boldsymbol{y}|} \, \phi_v^{\,\dagger}(\boldsymbol{x})\phi_v(\boldsymbol{x})\phi_{\mathrm{g}}^\dagger(\boldsymbol{y})\phi_{\mathrm{g}}(\boldsymbol{y}). \tag{37}$$

We have used our approximation of having the up and down quark wave functions being equal, so the sum of the contribution of the three quarks gives the single term $\phi_{\mathrm{g}}^\dagger \phi_{\mathrm{g}}$. A direct evaluation of this diagram for a state with principal quantum number n gives a result very close to $-m_l \alpha^2/n^2$, with the difference attributable to relativistic effects and the finite size of the proton built into our model. The associated counter term in Fig. 3(b) contributes

$$\Delta E_{\mathrm{X}} = \alpha \int \frac{\mathrm{d}\boldsymbol{x}}{x} \, \phi_v^{\,\dagger}(\boldsymbol{x})\phi_v(\boldsymbol{x}). \tag{38}$$

For the $2s_{1/2}$ state it has the value

$$\Delta E_{\mathrm{X}} = \frac{m_l \alpha^2}{\gamma\sqrt{8(1+\gamma)}}, \tag{39}$$

where $\gamma \equiv \sqrt{1 - (Z\alpha)^2}$.

Comparing the sum of ΔE_{1C} and ΔE_X to $E^{(1)}$ [Eq. (5)], one sees that it is exactly reproduced by the field-theory expression. However, because we now have a specific model for $\rho(\boldsymbol{x})$, we do not make the approximations made in the QM treatment and instead numerically evaluate it. We find

$$E^{(1)} = 2.278\,68 \times 10^{-11} \text{ a.u.} \quad \text{[hydrogen]}$$
$$E^{(1)} = 2.006\,26 \times 10^{-4} \text{ a.u.} \quad \text{[muonic hydrogen]}, \tag{40}$$

where all digits are significant. The root-mean-square charge radius r_p for $R = 1.2$ fm is

$$r_p = 0.728\,966\,R$$
$$= 0.874\,760 \text{ fm}. \tag{41}$$

We emphasize that this is not meant to be a prediction of the proton's rms radius, it is simply the static-well result when $R = 1.2$ fm. However, if we use this in the standard nonrelativistic expression for the finite size effect in hydrogen given in Eq. (6) we get

$$E_0^{(1)} = 2.277\,15 \times 10^{-11} \text{ a.u.} \quad \text{[hydrogen]}$$
$$E_0^{(1)} = 2.013\,00 \times 10^{-4} \text{ a.u.} \quad \text{[muonic hydrogen]}, \tag{42}$$

which differ from the exact result by $0.07\,\%$ and $0.34\,\%$ respectively. Thus we see that the calculation reproduces the bulk of the nonrelativistic expression for the effect of finite nuclear size on $2s_{1/2}$ energy levels. In the following, while the basic parameter of the static-well model is the well radius R, we use Eq. (41) to replace it by $1.3718\,r_p$ in all formulas dependent on R.

As we have a complete model of the charge distribution, these small deviations can be attributed to higher moments and relativistic effects. By carrying out the calculation for a range of R around 1.2 fm, we find the fits

$$E^{(1)}(\tilde{r}_p) = [2.977\,91 \times 10^{-11}\,\tilde{r}_p^{2\gamma} - 6.188\,69 \times 10^{-16}\,\tilde{r}_p^3]\,\text{a.u.} \tag{43}$$

for hydrogen and

$$E^{(1)}(\tilde{r}_p) = [2.631\,70 \times 10^{-4}\,\tilde{r}_p^{2\gamma} - 1.126\,29 \times 10^{-6}\tilde{r}_p^3]\,\text{a.u.} \tag{44}$$

for muonic hydrogen, where $\tilde{r}_p$ denotes r_p in units of fermis (femtometers).

We first note that the coefficients of the first and second terms for hydrogen increase by close to a factor of $(m_\mu/m_e)^3$ and $(m_\mu/m_e)^4$ respectively for muonic hydrogen, consistent with the dependence on m_l shown in Eqns. (6) and (12). The coefficients agree at a level of the order of one tenth of a percent. We originally attempted the fit with a quadratic term in $\tilde{r}_p$ instead of a term with the exponent 2γ, but were forced to use the latter form for hydrogen to get a proper fit. (The effect is less important for muonic hydrogen). In fact, it is known that the actual dependence of leading finite-size correction on $\tilde{r}_p$ is not the nonrelativistic quadratic form, but instead the relativistic form used above, as shown in Ref. [13]. In perturbation theory, the leading effect of the fractional power is a correction given by the Taylor expansion of $\tilde{r}_p^{2\gamma-2}$, which leads to a logarithmic term of relative order $(Z\alpha)^2 \ln \tilde{r}_p$.

V. SCREENING OF THE PROTON SELF ENERGY

As mentioned in the introduction, the proton electromagnetic self energy has contributions from the Feynman diagrams of Fig. 2. Before discussing how these diagrams are modified when the lepton interacts with the proton, which can be thought of as the Lamb shift of the proton, we mention another Lamb shift related term. This other effect, while negligible for hydrogen because it is of relative order $(m_r/M_N)^2$, makes a small contribution for muonic hydrogen, and is not suppressed at all for positronium, accounting for the self energy of the positron in that system. It was first derived by Fulton and Martin [14], and is given by

$$E_{\text{SEN}} = \frac{4\alpha^5}{3\pi n^3} \frac{m_r^3}{m_N^2} \left[\ln\left(\frac{m_N}{m_r\alpha^2}\right) \delta_{l0} - \ln k_0(n,l) \right], \tag{45}$$

where $\ln k_0(n,l)$ is the Bethe logarithm. This recoil effect, which shifts the $2s_{1/2}$ energy in muonic hydrogen by 0.010 meV, is not included in our approach.

An isolated proton can of course emit and reabsorb a photon, giving rise to the electromagnetic self energy of the proton just mentioned. This contributes to the mass of the proton, but when the proton is in a bound state an additional shift arises, described in lowest order by the Feynman diagrams in Figs. 4(a) and 4(b). We note in passing

that these diagrams do not have an analog in the QM treatment, as they involve internal electromagnetic interactions in the proton. In this paper we restrict our attention to the second of these diagrams, which we refer to as exchange corrections to the EM self energy of the proton and label as $\Delta E_{\mathrm{ex}}(\mathrm{pLS})$. This is justified by the behavior of the lowest-order proton electromagnetic self energy, where the size of the exchange term and the quark self energy are of the same magnitude. The photon propagators are both taken to be Coulomb propagators, and it is straightforward to show that this set of diagrams gives the energy shift

$$\Delta E_{\mathrm{ex}}(\mathrm{pLS}) = -2\alpha^2 \frac{\tilde{q}_i \tilde{q}_j^2}{16\pi^2} \int \frac{\mathrm{d}\boldsymbol{x}\, \mathrm{d}\boldsymbol{y}\, \mathrm{d}\boldsymbol{z}\, \mathrm{d}\boldsymbol{w}}{|\boldsymbol{x}-\boldsymbol{y}||\boldsymbol{w}-\boldsymbol{z}|} \psi^\dagger{}_v(\boldsymbol{w})\psi_v(\boldsymbol{w})$$
$$\times \sum_n \frac{1}{\epsilon_{\mathrm{g}} - \epsilon_n} \left\langle p \left| : \psi^\dagger{}_i(\boldsymbol{x})\psi_i(\boldsymbol{x})\psi^\dagger{}_j(\boldsymbol{y})\phi_n(\boldsymbol{y})\phi_n^\dagger(\boldsymbol{z})\psi_j(\boldsymbol{z}) : \right| p \right\rangle. \tag{46}$$

In this equation i and j are understood to be summed over the two flavors and appropriate sums over color indices are implicit; $\tilde{q}_i$ is the charge of the up or down quark in units of e depending on whether $i = 1$ or 2 respectively; ψ_i, ψ_j, and their adjoints are field operators, but ϕ_n and its adjoint are wavefunctions, with the sum over n going over all allowed values of angular momentum, κ_n and μ_n, and the positive- and negative-energy states associated with κ_n. For two Coulomb photons, one can show that only $\kappa_n = -1$ yields a non-zero contribution. After taking the normal-ordered product of the quark fields between the spin up wave function of the proton and noting the integrations over angles are all elementary, one is left with the sum

$$\Delta E_{\mathrm{ex}}(\mathrm{pLS}) = \frac{8}{9}\alpha^2 \sum_{[n]} \frac{1}{\epsilon_{\mathrm{g}} - \epsilon_n} \int_0^R \mathrm{d}x\, x^2 R_{\mathrm{gg}}(x) \int_0^R \mathrm{d}y\, y^2 R_{\mathrm{g}n}(y)$$
$$\int_0^R \mathrm{d}z\, z^2 R_{n\mathrm{g}}(z) \int_0^\infty \mathrm{d}w\, w^2 R_{vv}(w) \frac{1}{\max(x,y)} \frac{1}{\max(z,w)}, \tag{47}$$

where $[n]$ denotes summation over all s-states except the $1s$ state, and

$$R_{ij}(x) \equiv f_{1i}(x)f_{1j}(x) + f_{2i}(x)f_{2j}(x). \tag{48}$$

We find, using finite basis sets to carry out the sum over $[n]$, that

$$\Delta E_{\mathrm{ex}}(\mathrm{pLS}) = 0.5 \times 10^{-3} \text{ meV}. \tag{49}$$

The smallness of this effect is related to the fact the integral over z in Eq. (47) is

$$\int_0^R \mathrm{d}z\, z^2 R_{n\mathrm{g}}(z) \frac{1}{\max(z,w)}, \tag{50}$$

which vanishes when $w > R$ from the orthogonality of the radial wave functions. This restricts the muon wave function to lie within the nucleus, which gives a large suppression factor that scales as $(R/a_0)^3$.

This same suppression factor should make the diagram of Fig. 4(a), which is more difficult to evaluate, numerically unimportant. However, an interesting application of our approach would be the calculation of vacuum polarization. This was shown in Ref. [4] to vanish for a free proton, but when bound in an atom the arguments for its vanishing no longer apply, and in fact this should correspond to the effect of hadronic vacuum polarization, which is treated as a small effect, estimated in Ref. [5] to be 0.011 meV. However, we are not aware of any direct calculation of this term with zero-mass quarks, and will discuss how such a calculation could be carried out in the conclusions section.

Before turning to two-photon effects, we give more details about the use of finite basis sets. As described in Ref. [16], atomic finite basis set calculations are carried out in a well much larger than the atom, but with the same boundary conditions as used for the quarks. We continue to use an atomic basis set appropriate for hydrogen, but add a second basis set for the quarks, which is obtained by simple modifications of the atomic code, involving changing the fermion mass to zero, eliminating the potential, and changing from atomic units to MeV-fm units. Atomic grids are created on an exponential grid of the form $r(i) = r_0 \left[e^{h(i-1)} - 1 \right]$. We use the same grid for both quark and lepton wavefunctions. This is done by choosing parameters such that if, for example, a 1000 point grid were used for the atom, the two hundredth point would be at $r = 1.2$ fm, so that the quark wave function would be put on a 200 point grid that matched the atomic grid, though of course the quark wave function vanishes for $i > 200$. Several grids were used to test numerical stability. As is also the case for leptons, a complete set of positive and negative energy states result for each possible value of κ_n, in this case N positive energy s-states and N negative energy s-states, with a typical value of N being 50. For leptons the effect of the negative-energy states is generally very small, entering at the order of the Lamb shift. However, for quarks they play a more important role.

VI. TWO-PHOTON EXCHANGE

We now turn our attention to diagrams shown in Fig. 5. In this section we will show that they in part reproduce the second-order perturbation theory expression for $E^{(2)}$, Eq. (13) in Section II, but have in addition extra terms we identify as proton polarizability. To compare with individual diagrams, it is useful to employ Eq. (4) to represent δV in terms of $\rho - \delta$, which yields four terms for Eq. (13):

$$E_{\delta\delta}^{(2)} = \alpha^2 \int \mathrm{d}\boldsymbol{x}\, \mathrm{d}\boldsymbol{y}\, \phi_v^\dagger(\boldsymbol{x}) \frac{1}{|\boldsymbol{x}|} \sum_{m \neq v} \frac{\phi_m(\boldsymbol{x})\, \phi_m^\dagger(\boldsymbol{y})}{\epsilon_v - \epsilon_m} \frac{1}{|\boldsymbol{y}|}\, \phi_v(\boldsymbol{y}), \tag{51}$$

$$E_{\delta\rho}^{(2)} = -\alpha^2 \int \mathrm{d}\boldsymbol{x}\, \mathrm{d}\boldsymbol{y}\, \mathrm{d}\boldsymbol{w}\, \phi_v^\dagger(\boldsymbol{x}) \frac{1}{|\boldsymbol{x}|} \sum_{m \neq v} \frac{\phi_m(\boldsymbol{x})\, \phi_m^\dagger(\boldsymbol{y})}{\epsilon_v - \epsilon_m} \frac{\rho(\boldsymbol{w})}{|\boldsymbol{y} - \boldsymbol{w}|}\, \phi_v(\boldsymbol{y}), \tag{52}$$

$$E_{\rho\delta}^{(2)} = -\alpha^2 \int \mathrm{d}\boldsymbol{x}\, \mathrm{d}\boldsymbol{y}\, \mathrm{d}\boldsymbol{z}\, \phi_v^\dagger(\boldsymbol{x}) \frac{\rho(\boldsymbol{z})}{|\boldsymbol{x} - \boldsymbol{z}|} \sum_{m \neq v} \frac{\phi_m(\boldsymbol{x})\, \phi_m^\dagger(\boldsymbol{y})}{\epsilon_v - \epsilon_m} \frac{1}{|\boldsymbol{y}|}\, \phi_v(\boldsymbol{y}), \tag{53}$$

and

$$E_{\rho\rho}^{(2)} = \alpha^2 \int \mathrm{d}\boldsymbol{x}\, \mathrm{d}\boldsymbol{y}\, \mathrm{d}\boldsymbol{z}\, \mathrm{d}\boldsymbol{w}\, \phi_v^\dagger(\boldsymbol{x}) \frac{\rho(\boldsymbol{z})}{|\boldsymbol{x} - \boldsymbol{z}|} \sum_{m \neq v} \frac{\phi_m(\boldsymbol{x})\, \phi_m^\dagger(\boldsymbol{y})}{\epsilon_v - \epsilon_m} \frac{\rho(\boldsymbol{w})}{|\boldsymbol{y} - \boldsymbol{w}|}\, \phi_v(\boldsymbol{y}). \tag{54}$$

The simplest diagram, Fig. 5(a), is easily shown to give $E_{\delta\delta}^{(2)}$. The diagrams of Fig. 5(b) and its complex conjugate give $E_{\delta\rho}^{(2)}$ and $E_{\rho\delta}^{(2)}$ if we identify $\rho(\boldsymbol{x}) = \rho_{\mathrm{g}}(\boldsymbol{x})$ as in the treatment of one-photon exchange. This leaves only $E_{\rho\rho}^{(2)}$ to be accounted for. In general one contribution to it comes from Fig. 5(c), given by

$$\Delta E_2(ij) = \alpha^2 \tilde{q}_i\, \tilde{q}_j \sum_m \int \frac{\mathrm{d}\boldsymbol{x}\, \mathrm{d}\boldsymbol{y}\, \mathrm{d}\boldsymbol{z}\, \mathrm{d}\boldsymbol{w}}{|\boldsymbol{x} - \boldsymbol{z}||\boldsymbol{y} - \boldsymbol{w}|} \frac{\phi_v^\dagger(\boldsymbol{x})\phi_m(\boldsymbol{x})\phi_m^\dagger(\boldsymbol{y})\phi_v(\boldsymbol{y})}{\epsilon_v - \epsilon_m}$$
$$\times \left\langle p \left| : \psi_i^\dagger(\boldsymbol{z})\psi_i(\boldsymbol{z})\psi_j^\dagger(\boldsymbol{w})\psi_j(\boldsymbol{w}) : \right| p \right\rangle, \tag{55}$$

where the definition of $\tilde{q}_i$ is the same as in Sec. V. The various contributions to this term happen to sum to zero for the proton in our model, but we note they would not were we considering the neutron, or if we were taking the up and down quark wave functions to be different.

The final two diagrams, 5(d) and 5(e), are referred to as the ladder (L) and crossed ladder (XL) respectively. The closed loop in these diagrams is associated with an integration over a virtual energy. Because in this paper we consider only two-Coulomb photon exchange, the analysis of the loop integral is considerably simpler than the case where the photon propagators have energy dependence. That complication was encountered in the full Feynman gauge analysis of ladder and crossed ladder diagrams in excited states of helium-like ions [3], upon which the present calculation is patterned. Issues involved in carrying out the full calculation will be discussed in the conclusion. In this simpler case we can carry out the integral over the timelike component of the loop momentum with Cauchy's theorem, which requires identifying the poles coming from the propagators. We partition the lepton and quark propagators into positive and negative energy parts, which could lead to four contributions for each diagram, but the position of the poles is such that only two contributions fail to vanish. The surviving terms are

$$\Delta E_{\mathrm{L}}(++) = \tilde{q}_i^{\,2}\alpha^2 \int \frac{\mathrm{d}\boldsymbol{x}\, \mathrm{d}\boldsymbol{y}\, \mathrm{d}\boldsymbol{z}\, \mathrm{d}\boldsymbol{w}}{|\boldsymbol{x} - \boldsymbol{z}||\boldsymbol{y} - \boldsymbol{w}|} \sum_{m_+ n_+} \frac{\phi_v^\dagger(\boldsymbol{x})\phi_m(\boldsymbol{x})\phi_m^\dagger(\boldsymbol{y})\phi_v(\boldsymbol{y})}{\epsilon_v + \epsilon_{\mathrm{g}} - \epsilon_m - \epsilon_n}$$
$$\left\langle p \left| : \psi_{q_i}^\dagger(\boldsymbol{z})\psi_n(\boldsymbol{z})\psi_n^\dagger(\boldsymbol{w})\psi_{q_i}(\boldsymbol{w}) : \right| p \right\rangle \tag{56}$$

and

$$\Delta E_{\mathrm{L}}(--) = -\tilde{q}_i^{\,2}\alpha^2 \int \frac{\mathrm{d}\boldsymbol{x}\, \mathrm{d}\boldsymbol{y}\, \mathrm{d}\boldsymbol{z}\, \mathrm{d}\boldsymbol{w}}{|\boldsymbol{x} - \boldsymbol{z}||\boldsymbol{y} - \boldsymbol{w}|} \sum_{m_- n_-} \frac{\phi_v^\dagger(\boldsymbol{x})\phi_m(\boldsymbol{x})\phi_m^\dagger(\boldsymbol{y})\phi_v(\boldsymbol{y})}{\epsilon_v + \epsilon_{\mathrm{g}} - \epsilon_m - \epsilon_n}$$
$$\left\langle p \left| : \psi_{q_i}^\dagger(\boldsymbol{z})\psi_n(\boldsymbol{z})\psi_n^\dagger(\boldsymbol{w})\psi_{q_i}(\boldsymbol{w}) : \right| p \right\rangle \tag{57}$$

for the ladder diagram, and

$$\Delta E_{\text{XL}}(+-) = \tilde{q_i}^2 \alpha^2 \int \frac{\mathrm{d}\boldsymbol{x}\,\mathrm{d}\boldsymbol{y}\,\mathrm{d}\boldsymbol{z}\,\mathrm{d}\boldsymbol{w}}{|\boldsymbol{x}-\boldsymbol{w}||\boldsymbol{y}-\boldsymbol{z}|} \sum_{m_+ n_+} \frac{\phi_v^\dagger(\boldsymbol{x})\phi_m(\boldsymbol{x})\phi_m^\dagger(\boldsymbol{y})\phi_v(\boldsymbol{y})}{\epsilon_{\text{g}} - \epsilon_v + \epsilon_m - \epsilon_n}$$
$$\left\langle p\left|:\psi_{q_i}^\dagger(\boldsymbol{z})\psi_n(\boldsymbol{z})\psi_n^\dagger(\boldsymbol{w})\psi_{q_i}(\boldsymbol{w}):\right|p\right\rangle \tag{58}$$

and

$$\Delta E_{\text{XL}}(-+) = -\tilde{q_i}^2 \alpha^2 \int \frac{\mathrm{d}\boldsymbol{x}\,\mathrm{d}\boldsymbol{y}\,\mathrm{d}\boldsymbol{z}\,\mathrm{d}\boldsymbol{w}}{|\boldsymbol{x}-\boldsymbol{w}||\boldsymbol{y}-\boldsymbol{z}|} \sum_{m_- n_-} \frac{\phi_v^\dagger(\boldsymbol{x})\phi_m(\boldsymbol{x})\phi_m^\dagger(\boldsymbol{y})\phi_v(\boldsymbol{y})}{\epsilon_{\text{g}} - \epsilon_v + \epsilon_m - \epsilon_n}$$
$$\left\langle p\left|:\psi_{q_i}^\dagger(\boldsymbol{z})\psi_n(\boldsymbol{z})\psi_n^\dagger(\boldsymbol{w})\psi_{q_i}(\boldsymbol{w}):\right|p\right\rangle \tag{59}$$

for the crossed ladder. The relative minus sign between the two ladder and the two crossed ladder terms comes from closing the contour in different ways, and we note that the Coulomb propagators are different for the ladder and crossed ladder diagrams. In the following we will give formulas only for $\Delta E_{\text{L}}(++)$ and $\Delta E_{\text{XL}}(-+)$ as the other terms differ from these only by an overall minus sign and a reversed role of positive and negative energy states.

A.   Elastic contribution

At this point we divide the sum over intermediate quark states into a part with $n = \text{g}$, which leaves the proton unchanged and corresponds to elastic scattering, and the remaining part, corresponding to inelastic scattering, which gives the polarizability contribution. We now show that the elastic term contains $E_{\rho\rho}^{(2)}$. As ϵ_n is a positive energy, only $\Delta E_{\text{L}}(++)$ and $\Delta E_{\text{XL}}(-+)$ contribute. Because the quark states are now all s-states, the angular-momentum dependence is particularly simple. The Coulomb propagators can be simplified with the replacements

$$\frac{1}{|\boldsymbol{x}-\boldsymbol{z}|} \to \frac{1}{r_{1a}}$$
$$\frac{1}{|\boldsymbol{y}-\boldsymbol{w}|} \to \frac{1}{r_{2a}} \tag{60}$$

with $r_{1a} = \max(|\boldsymbol{x}|,|\boldsymbol{z}|)$, $r_{2a} = \max(|\boldsymbol{y}|,|\boldsymbol{w}|)$. (For later use we define $r_{1b} = \min(|\boldsymbol{x}|,|\boldsymbol{z}|)$, $r_{2b} = \min(|\boldsymbol{y}|,|\boldsymbol{w}|)$.) Integration over angles then yields

$$\Delta E_L(++) = \alpha^2 \int \mathrm{d}V \frac{1}{r_{1a} r_{2a}} \sum_{m_+} \frac{R_{vm}(x) R_{mv}(y) R_{\text{gg}}(z) R_{\text{gg}}(w)}{\epsilon_v - \epsilon_m}, \tag{61}$$

with m being forced to be an s state. We have introduced the shorthand

$$\int \mathrm{d}V \equiv \int_0^\infty \mathrm{d}x\,x^2 \int_0^\infty \mathrm{d}y\,y^2 \int_0^R \mathrm{d}z\,z^2 \int_0^R \mathrm{d}w\,w^2. \tag{62}$$

Because $R_{\text{gg}}(w)/4\pi = \rho_{\text{g}}(w)$, this reproduces the part of $E_{\rho\rho}^{(2)}$ in which the electron propagator involves sums over positive energy states. In order to include the part with negative energy states the crossed ladder must be considered. The minus sign mentioned above is needed for the energy denominators to match, and the fact that $\rho(\boldsymbol{z})\rho(\boldsymbol{w})$ is symmetric under interchange of $\boldsymbol{z}$ and $\boldsymbol{w}$ is also needed. Thus part of the ladder and crossed ladder diagrams together with the other diagrams of Fig. 5 simply reproduce second-order perturbation theory with a particular form for the charge distribution of the proton.

We evaluated these terms numerically as a test of the coding, since the QM treatment yields a nonrelativistic (NR) limit for comparison. The result for muonic hydrogen is

$$E_{2s}^{(2)} = -3.948 \times 10^{-7} \text{ a.u.,} \tag{63}$$

which is within $4\,\%$ of the NR formula. We recall that formula has a mixture of the Zemach term and a $\langle r^3 \rangle$ term, where the latter cancels part of the one-loop result.

B. Proton polarizability

We now turn to the evaluation of the remaining parts of the ladder and crossed ladder. The quark propagator is treated in the same manner as described in Sec. V. The feature of the basis set mentioned in that section, whereby it automatically breaks into a positive and a negative energy part, makes separation of the various diagrams a simple matter. We begin with the case where $\kappa_m = \kappa_n = -1$, but where we do not allow the intermediate quark to be in the ground state. The result for the ladder is $0.000\,5$ meV, and is almost completely cancelled by the crossed ladder, which contributes $-0.000\,5$ meV, making this channel completely negligible.

In order to treat higher partial waves we must now specify the spin state of the atom. Polarizability is important only for the $2s_{1/2}$ state, which of course can be a triplet or singlet state once the spin of the proton is considered. For one-Coulomb-photon exchange these states have the same energy, as hyperfine splitting comes from transverse photon exchange, which is not treated here. However, with two-photon exchange, even when both are Coulomb photons, the triplet and singlet energies differ except for the $l = 0$ partial wave discussed above. We therefore present in the following formulas for the energy levels of the $2s_{1/2}$ singlet and triplet.

While each Coulomb propagator has its own partial wave expansion, leading in general to a double sum over l_1 and l_2, the fact that the quarks are all in s-states leads to the simplification that these values are equal, $l_1 = l_2 \equiv l$. Another simplification is that for a given l, only κ_m and κ_n values associated with that value give a non-vanishing contribution. We define angular factors $A_l(\kappa_m, \kappa_n)$ for the ladder and $B_l(\kappa_m, \kappa_n)$ for the crossed ladder diagrams, which are rational fractions resulting from the integrations over angles and sums over magnetic quantum numbers, tabulated in Table I for $l = 1$ and $l = 2$. Both the triplet and singlet state results are given, though in this paper we are only interested in fine structure. The case $l = 1$ corresponds to the dominant dipole transition. In terms of these coefficients, the formula for the ladder is

$$\Delta E_L(++) = \alpha^2 \sum_l \int dV \, \frac{r_{1b}^l r_{2b}^l}{r_{1a}^{l+1} r_{2a}^{l+1}} \sum_{m_+ n_+} A_l(\kappa_m, \kappa_n) \frac{R_{vm}(x) R_{mv}(y) R_{gn}(z) R_{ng}(w)}{\epsilon_v + \epsilon_g + \epsilon_n - \epsilon_m} \tag{64}$$

and for the crossed ladder is

$$\Delta E_X(+-) = \alpha^2 \sum_l \int dV \, \frac{r_{3b}^l r_{4b}^l}{r_{3a}^{l+1} r_{4a}^{l+1}} \sum_{m_+ n_-} B_l(\kappa_m, \kappa_n) \frac{R_{vm}(x) R_{mv}(y) R_{gn}(z) R_{ng}(w)}{\epsilon_v - \epsilon_g + \epsilon_n - \epsilon_m}, \tag{65}$$

where $r_{3a} = \max(|\boldsymbol{x}|, |\boldsymbol{w}|), r_{3b} = \min(|\boldsymbol{x}|, |\boldsymbol{w}|)$ and $r_{4a} = \max(|\boldsymbol{y}|, |\boldsymbol{z}|), r_{4b} = \min(|\boldsymbol{y}|, |\boldsymbol{z}|)$.

		$l = 1$						$l = 2$			
κ_m	κ_n	A_1(T)	A_1(S)	B_1(T)	B_1(S)	κ_m	κ_n	A_2(T)	A_2(S)	B_2(T)	B_2(S)
1	1	17/729	57/729	37/729	17/729	2	2	26/1125	66/1125	46/1125	26/1125
1	−2	64/729	24/729	44/729	64/729	2	−3	64/1125	24/1125	44/1125	64/1125
−2	1	64/729	24/729	44/729	64/729	−3	2	64/1125	24/1125	44/1125	64/1125
−2	−2	98/729	138/729	118/729	98/729	−3	−3	71/1125	111/1125	91/1125	71/1125

TABLE I. Angular coefficient factors for the allowed values of κ_m, κ_n for $l = 1$ and $l = 2$. Factors of A_l are for the ladder diagram; factors of B_l are for the crossed ladder. "T" refers to the triplet atomic state, while "S" refers to the singlet.

These can be evaluated with the techniques described above with only simple changes, as the spline basis set contains all values of κ needed and the radial integrals over r_b^l/r_a^{l+1} are evaluated with techniques valid for arbitrary l. The main numerical problem was ensuring that the typical rapid convergence of splines in atomic physics carried over to this problem. The calculation shows that the effect of the $l = 2$ channel is very small, with almost the entire effect of polarizability coming from the $l = 1$ dipole channel, which shifts the $2s_{1/2}$ energy down by 0.026 meV. This leads to our main polarizability result for the splitting,

$$E(2s_{1/2} - 2p_{3/2}) = 0.026 \, \text{meV}, \tag{66}$$

consistent with the results from dispersion relation analyses, as will be discussed in the conclusions.

VII. STATIC POLARIZABILITIES

One of the basic electromagnetic properties of the proton is its static polarizability, which has an electric and a magnetic component. We concentrate on the static electric polarizability, which is given by the Particle Data Group

(PDG) as

$$\alpha_{\mathrm{p}} = 12.0(6) \times 10^{-4} \ \mathrm{fm}^3. \tag{67}$$

While this value is extracted from Compton scattering data together with dispersion theory arguments [19], in the static-well model the lowest-order expression comes from the diagram of Fig. 6, where the line with a cross indicates a constant electric field with magnitude E_{ext}. The energy shift is related to the static electric polarizability through

$$\Delta E_\alpha = -\frac{1}{2} \alpha_{\mathrm{p}} E_{\mathrm{ext}}^2. \tag{68}$$

We note two similar calculations using the closely related MIT bag model [20], [21] have been presented, but detailed comparison with their results is not possible. A factor of 4π has been absorbed into the external field.

The basic equation for the energy shift of a proton in the presence of a constant electric field described by the potential $\phi(\boldsymbol{r}) = -E_{\mathrm{ext}} x_3$ is

$$\Delta E_\alpha = \tilde{q}_i^2 E_{\mathrm{ext}}^2 \sum_n \frac{1}{\epsilon_{\mathrm{g}} - \epsilon_n} \int \mathrm{d}\boldsymbol{x} \, \mathrm{d}\boldsymbol{y} \, \langle p | : \psi_{q_i}^\dagger(\boldsymbol{x}) x_3 \psi_n(\boldsymbol{x}) \psi_n^\dagger(\boldsymbol{y}) y_3 \psi_{q_i}(\boldsymbol{y}) : | p \rangle \tag{69}$$

which reduces to

$$\Delta E_\alpha = \frac{\alpha}{9} E_{\mathrm{ext}}^2 \sum_n \int \mathrm{d}\boldsymbol{x} \, \mathrm{d}\boldsymbol{y} \, \frac{7 \phi_a^\dagger(\boldsymbol{x}) x_3 \phi_n(\boldsymbol{x}) \phi_n^\dagger(\boldsymbol{y}) y_3 \phi_a(\boldsymbol{y}) + 2 \phi_b^\dagger(\boldsymbol{x}) x_3 \phi_n(\boldsymbol{x}) \phi_n^\dagger(\boldsymbol{y}) y_3 \phi_b(\boldsymbol{y})}{\epsilon_{\mathrm{g}} - \epsilon_n}. \tag{70}$$

For this case the orientation of the quark spin does not matter, so the expression simplifies to

$$\alpha_{\mathrm{p}} = -2 \sum_n \frac{1}{\epsilon_{\mathrm{g}} - \epsilon_n} \int \mathrm{d}\boldsymbol{x} \, \mathrm{d}\boldsymbol{y} \, \phi_{\mathrm{g}}^\dagger(\boldsymbol{x}) x_3 \phi_n(\boldsymbol{x}) \phi_n^\dagger(\boldsymbol{y}) y_3 \phi_{\mathrm{g}}(\boldsymbol{y}), \tag{71}$$

where we have now isolated the factor $-\frac{1}{2} E_{\mathrm{ext}}^2$ to give the formula in terms of α_{p}. We emphasize at this point that this is a field theoretic derivation, and that the sum over n is complete, including negative-energy states.

Introducing the notation [see Eq. (48)]

$$r_{ij} \equiv \int_0^R \mathrm{d}x \, x^3 \, R_{ij}(x), \tag{72}$$

after integration over coordinate angles we find

$$\alpha_{\mathrm{p}} = -\frac{2}{9} \sum_{\substack{n \\ \kappa_n = 1}} \frac{r_{\mathrm{g}n} r_{n\mathrm{g}}}{\epsilon_{\mathrm{g}} - \epsilon_n} - \frac{4}{9} \sum_{\substack{n \\ \kappa_n = -2}} \frac{r_{\mathrm{g}n} r_{n\mathrm{g}}}{\epsilon_{\mathrm{g}} - \epsilon_n}. \tag{73}$$

We calculated the two terms with basis set techniques. The most striking result found was that the $\kappa = 1$ channel vanishes. If one sums over only positive energy states one obtains a nonzero result, but inclusion of the negative energy states leads to an exact cancellation. This situation does not occur for the $\kappa = -2$ channel, which in our model is solely responsible for the proton static polarizability.

We also calculated α_{p} using a form for the quark propagator that does not rely on the spectral decomposition given in Eq. (33). After rewriting Eq. (71) as

$$\alpha_p = 2 \int \mathrm{d}\boldsymbol{x} \, \mathrm{d}\boldsymbol{y} \, \phi_{\mathrm{g}}^\dagger(\boldsymbol{x}) x_3 G_{\mathrm{q}}(\boldsymbol{x}, \boldsymbol{y}; \epsilon_{\mathrm{g}}) y_3 \phi_{\mathrm{g}}(\boldsymbol{y}), \tag{74}$$

we use the fact that the quark Green function satisfies the differential equation

$$(-\mathrm{i}\boldsymbol{\alpha} \cdot \boldsymbol{\nabla}_{\boldsymbol{x}} + \beta m_{\mathrm{q}} - \epsilon_{\mathrm{g}}) G_{\mathrm{q}}(\boldsymbol{x}, \boldsymbol{y}; \epsilon_{\mathrm{g}}) = \delta^3(\boldsymbol{x} - \boldsymbol{y}) \tag{75}$$

with appropriate boundary conditions. Without those conditions this is the same equation that a free fermion Green function satisfies, and a simple modification of the well-known partial-wave expansion of the latter propagator can be made to solve for the quark propagator. We illustrate this for the Green function of a massless quark with positive $\kappa = l$ and $x > y$, in which case

$$G_{\mathrm{q}}(\boldsymbol{x}, \boldsymbol{y}; \epsilon_{\mathrm{g}}) = \mathrm{i}\epsilon_{\mathrm{g}}^2 \sum_{\kappa\mu} \begin{pmatrix} [h_l(\epsilon_{\mathrm{g}} x) + A_l j_l(\epsilon_{\mathrm{g}} x)] \, \chi_{\kappa\mu}(\hat{\boldsymbol{x}}) \\ \mathrm{i} \, [h_{l-1}(\epsilon_{\mathrm{g}} x) + A_l j_{l-1}(\epsilon_{\mathrm{g}} x)] \, \chi_{-\kappa\mu}(\hat{\boldsymbol{x}}) \end{pmatrix}$$

$$\times \begin{pmatrix} j_l(\epsilon_{\mathrm{g}} y) \chi_{\kappa\mu}^\dagger(\hat{\boldsymbol{y}}) & -\mathrm{i} j_{l-1}(\epsilon_{\mathrm{g}} y) \chi_{-\kappa\mu}^\dagger(\hat{\boldsymbol{y}}) \end{pmatrix}. \tag{76}$$

The coefficients A_l are determined by the boundary condition. The fact that the propagator ranges over a finite volume allows the admixture of the solution proportional to A_l which is forbidden for a free propagator because of the boundary condition as $x \to \infty$. When $\kappa = 1$, the integrand in Eq. (74) includes the factor

$$\left(\begin{array}{cc} j_1(\epsilon_{\mathrm{g}} y)\chi^\dagger_{1\mu}(\hat{\boldsymbol{y}}) & -\mathrm{i} j_0(\epsilon_{\mathrm{g}} y)\chi^\dagger_{-1\mu}(\hat{\boldsymbol{y}}) \end{array} \right) \left(\begin{array}{c} j_0(\epsilon_{\mathrm{g}} y)\chi_{-1\mu}(\hat{\boldsymbol{y}}) \\ -\mathrm{i} j_1(\epsilon_{\mathrm{g}} y)\chi_{1\mu}(\hat{\boldsymbol{y}}) \end{array} \right) \tag{77}$$

which vanishes. An analogous factor on the left-hand-side when $x < y$ also vanishes. However, for $\kappa = -2$ there is no such cancellation, and using

$$A_1 = \frac{h_2(\epsilon_{\mathrm{g}} R) - h_1(\epsilon_{\mathrm{g}} R)}{j_2(\epsilon_{\mathrm{g}} R) - j_1(\epsilon_{\mathrm{g}} R)}, \tag{78}$$

we find the numerical result

$$\alpha_{\mathrm{p}} = 25.4 \times 10^{-4} \ \mathrm{fm}^3 \,. \tag{79}$$

The spectral decomposition discussed previously gives the same result, and we find that the sum is dominated by the first $p_{3/2}$ state, with higher-n positive-energy and negative-energy states entering at under one tenth of a percent. This result is a factor of two larger than the experimental value in Eq. (67). However, we note that the relation of the PDG result quoted to static polarizability determined from energy shifts involves some subtleties, discussed in [19] and more recently in [22].

VIII. CONCLUSIONS

In this paper we present an approach to the calculation of the effect of the electromagnetic structure of the proton on energy levels of muonic hydrogen that uses a simple bound-state model for the proton, with only one free parameter, the radius of the well, which we have chosen to be $R = 1.2$ fm. Once the formalism is set up, standard techniques of quantum field theory can be used to evaluate proton structure effects using this parameter, in contrast to the standard approach, which involves the analysis of forward photon-proton scattering. We do not claim our approach is better, only that it introduces a different way of looking at the problem.

We have considered only Coulomb photons in this paper. This is because our primary concern was in setting up the basic formalism, and testing it in the relatively tractable case of Coulomb photon exchange. To continue, while one could stay in the Coulomb gauge and introduce transverse photons, it is simpler to simply change to the Feynman gauge. Because the quarks all have the same energy, much of the work here is effectively already in the Feynman gauge, with $\gamma_\mu \cdots \gamma^\mu \to \gamma_0 \cdots \gamma_0$. Continuing the calculation to this more complete approach will allow the treatment of the interesting case of hyperfine splitting. The difficulties of proton structure are well known to be exacerbated in this case, with even ground-state hydrogen hfs uncertain at the sixth digit. Our approach should allow a direct calculation of what is often referred to as dynamic proton polarizability, as well as allowing a systematic treatment of other spin dependent effects that sometimes are difficult to disentangle. These calculations are complicated by the fact that the loop energy integral can no longer be evaluated with Cauchy's theorem. Instead one must carry out a Wick rotation to the imaginary axis and carry out the integral numerically. This rotation requires care because of the presence of poles and cuts in the complex plane, which leads to a number of extra terms.

We have shown that in our method a term, while extremely small, that can be thought of as the Lamb shift of the proton arises. The smallness of the effect had very much to do with the fact that all three quarks are taken to be in the $1s$ state, which limits the κ values allowed for the propagator. It is an interesting open question as to how this effect would change if corrections to the proton wave function involving non-s states were present, as they presumably are because of gluon exchange, but that is outside the scope of this paper.

We have shown that the one-photon diagrams together with the elastic part of the two-photon diagrams give the following contribution to the Lamb shift:

$$E_{\mathrm{fns}}(\text{non-recoil}) = \left[-7.161\,22\, \tilde{r}_{\mathrm{p}}^{2\gamma} + 0.046\,70\, \tilde{r}_{\mathrm{p}}^3 \right] \ \mathrm{meV}, \tag{80}$$

which is the sum of Eq. (44) and Eq. (63) with $\tilde{r}_{\mathrm{p}}^3$ factored out of the latter value. This was calculated without the large recoil corrections present in muonic hydrogen: multiplying the appropriate factors of $(m_{\mathrm{r}}/m_\mu)^3$ and $(m_{\mathrm{r}}/m_\mu)^4$ into the first and second terms, our result becomes

$$E_{\mathrm{fns}} = \left[-5.199\,5\, \tilde{r}_{\mathrm{p}}^{2\gamma} + 0.030\,5\, \tilde{r}_{\mathrm{p}}^3 \right] \ \mathrm{meV}. \tag{81}$$

The polarizability of the proton was calculated in a novel fashion. The basic result of this paper is that despite the difference in approach, a similarly small result is found. Specifically, again restoring recoil corrections by multiplying our result by $(m_{\rm r}/m_{\mu})^4$, we have found the proton polarizability correction

$$\Delta E_{\rm pol} = 0.017\,{\rm meV}. \tag{82}$$

While inclusion of transverse photons may lead to quantitative changes, we consider it unlikely that a qualitative change will result. We would expect this additional correction to be of relative order α, unlike in the case for two-photon exchange between two electrons bound by a high-Z nucleus where the correction is of relative order α^2. The difference arises from the fact that the "small" components of the highly-relativistic quark wave functions are of the same order as the "large" components, rather than being smaller by a factor of α.

We now compare our results with Ref. [7], where the formula

$$\Delta E_{\rm LS} = \left[206.0336(15) - 5.2275(10)\tilde{r}_{\rm p}^2\right]\,{\rm meV} + \Delta E_{\rm TPE} \tag{83}$$

corresponds to their Eq. (32), with the breakdown of $\Delta E_{\rm TPE}$ given in their Table I. Our quadratic term compares well when a term $-0.0275\,\tilde{r}_{\rm p}^2$ meV arising from radiative corrections to finite size, not included in our work, is removed [8]. As shown in Table II, which gives contributions of the shift of the $2s_{1/2}$ level to the $2s_{1/2} - 2p_{3/2}$ transition energy, the breakup of $\Delta E_{\rm TPE}$ involves three terms, a subtraction term $\Delta E^{\rm subt}$ that has no counterpart in our calculation, an inelastic contribution $\Delta E^{\rm inel}$, which is the proton polarizability effect, and an elastic term $\Delta E^{\rm el}$ corresponding to unexcited proton size effects. The elastic term is not entirely a two-photon contribution in our approach, because there is a partial cancellation between the one- and two-photon diagrams, as discussed in Sec. II. Here we identify the number in the table as that contribution beyond the term quadratic in $\tilde{r}_{\rm p}$ from the sum of one- and two-photon-exchange diagrams with unexcited proton states. This is just the second (cubic in $\tilde{r}_{\rm p}$) term in Eq. (81). The agreement of the results of our calculation with previous results is remarkably good in view of the wide difference in the methods.

Correction	Ref. [23]	Refs. [24, 25]	Ref. [26]	This work	Eqn.
$\Delta E^{\rm subt}$	$-0.005(2)$ meV	-0.002 meV	-0.002 meV		
$\Delta E^{\rm inel}$	$0.013(1)$ meV	0.014 meV	0.016 meV	0.017 meV	(82)
$\Delta E^{\rm el}$	$0.030(1)$ meV	0.023 meV	0.023 meV	0.020 meV	(81)
$\Delta E_{\rm TPE}$	$0.037(2)$ meV	0.035 meV	0.037 meV	0.037 meV	

TABLE II. Comparison of this work with previous calculations. See the text for an explanation of the entries

Perhaps the most interesting calculation left undone in this framework is vacuum polarization. This of course dominates the muonic hydrogen $2s_{1/2} - 2p_{3/2}$ splitting when an electron is in the vacuum polarization loop, but in our framework we could also put in the zero-mass quarks confined in the well into the loop. For an isolated proton, symmetry arguments [4] show that vacuum polarization vanishes, but once in an atom the arguments no longer hold, and a finite effect should be present. The standard approach is to introduce pion loops, in which case the previously mentioned very small "hadronic vacuum polarization" value of 0.011 meV results, but this approach is quite different. Such calculations are, however, particularly challenging because of the high degree of divergence present, which always presents difficulties for bound-state methods. We are investigating whether techniques that have proved useful in studying vacuum polarization effects in atoms [27], where careful grouping of angular momentum contributions allows an accurate treatment of highly-divergent terms, can be extended to this novel case.

[1] A. Chodos, R.L. Jaffe, K. Johnson, C.B. Thorn, and V.F. Weisskopf, Phys. Rev. D **9**, 3471 (1974).
[2] W. Furry, Phys. Rev. **81**, 115 (1951).
[3] P.J. Mohr and J. Sapirstein, Phys. Rev. A **62**, 052501 (2000)
[4] P.J. Mohr and J. Sapirstein, Phys. Rev. Lett. **54**, 514 (1985).
[5] R. Pohl *et. al.*, Nature **466**, 213 (2010); A. Antognini *et. al.*, *Science*, 339 (6618) (2013).

[6] R.J. Hill and G. Paz, Phys. Rev. D**82**, 113005 (2010).

[7] R. Pohl, R. Gilman, G.A. Miller, Pohl, and K. Pachucki, arXiv:1301.0905, (2013).

[8] A. Antognini, F. Kottmann, F. Biraben, P. Indelicato, F. Nez, and R. Pohl, Ann. Phys. (N.Y.) **331**, 127 (2013).

[9] P.J. Mohr, B.N. Taylor, and D.B. Newell, Rev. Mod. Phys. **84**, 1527 (2012).

[10] A.N. Artemyev, V.M. Shabaev, and V.A. Yerokhin, Phys. Rev. A **52**, 1884 (1995).

[11] J. Sapirstein and K.T. Cheng, Phys. Rev. A**83**, 012504 (2011).

[12] P. Beiersdorfer, A.L. Osterheld, J.H. Scofield, J.R. Crespo Lopez-Urrutia, and K. Widmann, Phys. Rev. Lett. **80**, 3022 (1998).

[13] P.J. Mohr, At. Data Nucl. Data Tables **29**, 453 (1983).

[14] T. Fulton and P.C. Martin. Phys. Rev. **95**, 811 (1954).

[15] K. Pachucki, Phys. Rev. A **52**, 1079 (1995).

[16] W.R. Johnson, S.A. Blundell, and J. Sapirstein, Phys. Rev. A **37**, 307 (1988).

[17] J. Sucher, Phys. Rev. **109**, 1010 (1958); M. Gell-Mann and F. Low, Phys. Rev. **84**, 350 (1951).

[18] S.A. Blundell, K.T. Cheng, and J. Sapirstein, Phys. Rev. A **55**, 1857 (1997).

[19] A.I. L'vov, Int. Jour. Mod. Phys. A **8**, 5267 (1993).

[20] A. Schafer, B. Muller, D. Vasak and W. Greiner, Phys. Lett. B**143**, 323 (1984).

[21] B. Hecking and G.F. Bertsch, Phys. Lett. B**99**, 237 (1981).

[22] R.J. Hill, Gabriel Lee, Gil Paz, and Mikhail P. Solon, arxiV:1212.4508 (2012).

[23] C. E. Carlson and M. Vanderhaeghen, Phys. Rev. A **84**, 020102 (2011).

[24] K. Pachucki, Phys. Rev. A **53**, 2092 (1996).

[25] K. Pachucki, Phys. Rev. A **60**, 3593 (1999).

[26] A. P. Martynenko, Yad. Fiz. **69**, 1344 (2006) [Phys. At. Nucl. **69**, 1309 (2006)].

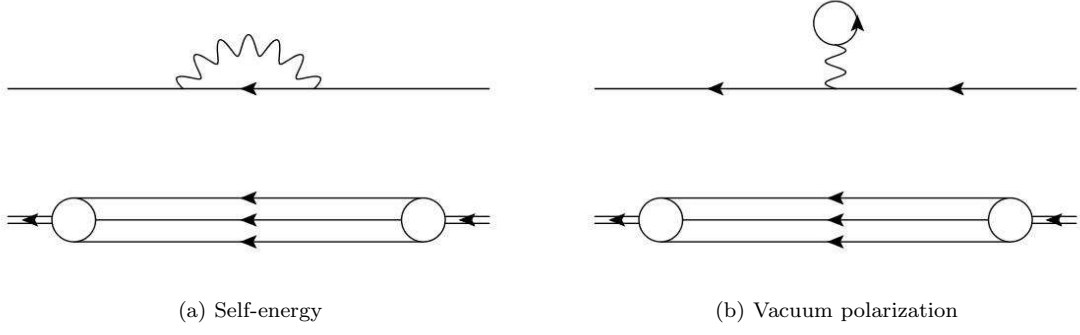[27] Gerhard Soff and Peter J. Mohr, Phys. Rev. A**38**, 5066 (1988).

(a) Self-energy

(b) Vacuum polarization

FIG. 1. The two diagrams contributing to the Lamb shift in the hydrogenic bound state.
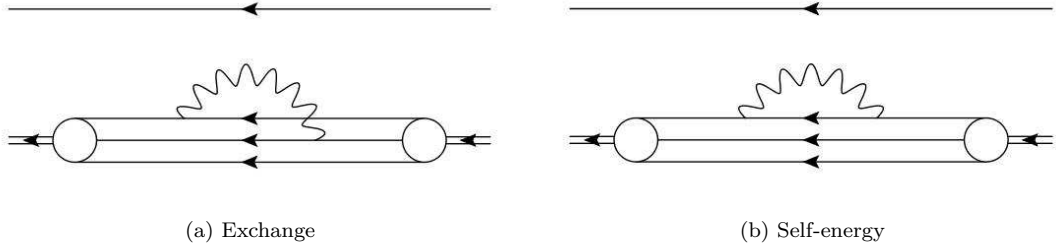

(a) Exchange

(b) Self-energy

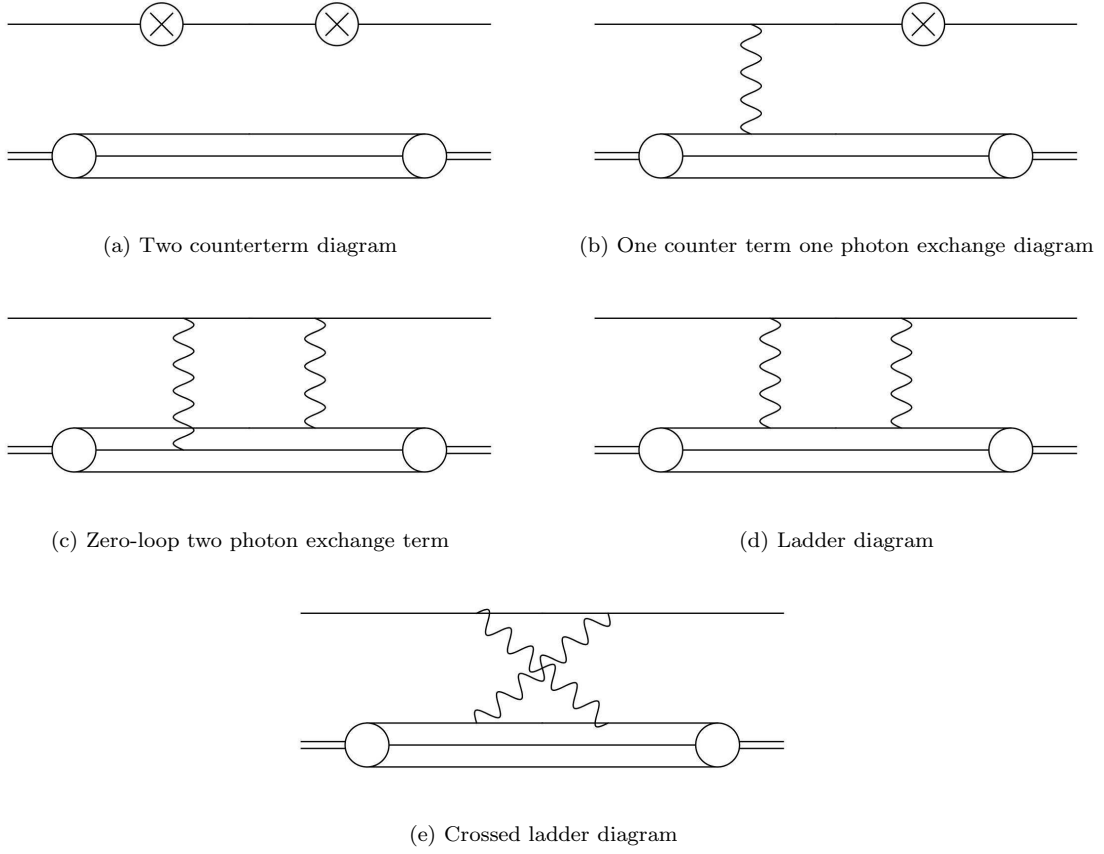FIG. 2. The two diagrams contributing to the Lamb shift in the proton bound state.

(a) One photon exchange between the lepton and a quark

(b) Counterterm contribution

FIG. 3. Order α contributions

(a) Proton Lamb shift vertex correction
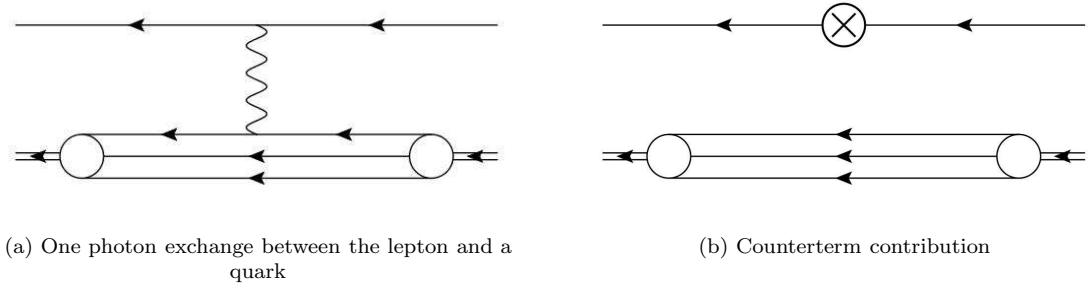
(b) Proton Lamb shift exchange correction
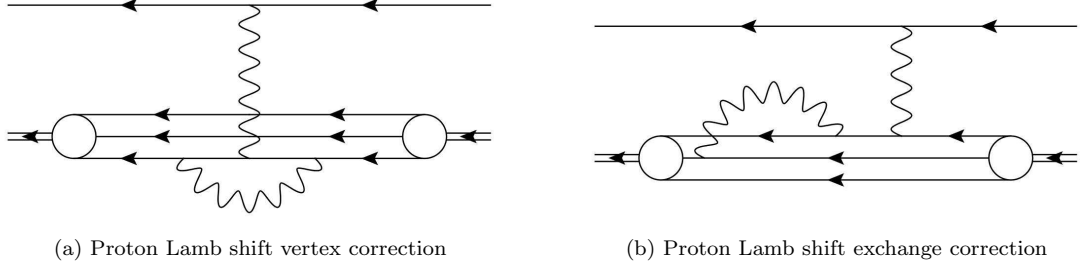
FIG. 4. Order α^2 corrections to proton Lamb shift

(a) Two counterterm diagram

(b) One counter term one photon exchange diagram

(c) Zero-loop two photon exchange term

(d) Ladder diagram

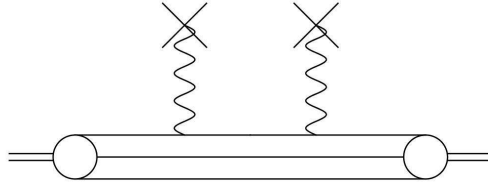(e) Crossed ladder diagram

FIG. 5. Order α^2 contributions to polarizability

FIG. 6. Diagram for static polarizability